Mon. Not. R. Astron. Soc. **000**, 000–000 (0000) Printed 1 February 2008 (MN LATEX style file v1.4)

A Nested Grid Particle-Mesh Code for High Resolution Simulations of Gravitational Instability in Cosmology

Randall J. Splinter⋆

Department of Physics and Astronomy,The University of Kansas, Lawrence, Kansas 66045 USA

Received 1995 March 15; in original form 1996 January 29

ABSTRACT

I describe a nested-grid particle-mesh (NGPM) code designed to study gravitational instability in three-dimensions. The code is based upon a standard PM code. Within the parent grid I am able to define smaller sub-grids allowing us to substantially extend the dynamical range in mass and length. I treat the fields on the parent grid as background fields and utilize a one-way interactive meshing. Waves on the coarse parent grid are allowed to enter and exit the subgrid, but waves from the subgrid are precluded from effecting the dynamics of the parent grid. On the parent grid the potential is computed using a standard multiple Fourier transform technique. On the subgrid I use a Fourier transform technique to compute the subgrid potential at high resolution. I impose quasi-isolated boundary conditions on the subgrid using the standard method for generating isolated boundary conditions, but rather than using the isolated Green function I use the Ewald method to compute a Green function on the subgrid which possesses the full periodicity of the parent grid. I present a detailed discussion of my methodology and a series of code tests.

Key words: cosmology – galaxies:clustering – numerical methods.

1 INTRODUCTION

Over the past decade N-body techniques have become the dominant method for studying the clustering of mass on large scales (see Efstathiou et al. 1985, or Hockney & Eastwood 1981). Direct particle-particle (PP) codes were the first n-body codes which were widely used, and they reached a remarkable state of development as discussed by Aarseth (1985). These codes tend to be very time consuming since each particle interacts with every other particle directly via a $1/r^2$ force. This technique allows for very high spatial resolution but at the expense of CPU time. As the particles clump the the small scale dynamics dominate and the CPU time required jumps dramatically. Treecodes are dramatically faster since they compute direct PP interactions only locally and the far field computations are performed using nodes of particles. These codes do not require a mesh and hence do not have the spatial resolution problems associated with the introduction of a grid. For both of these codes the small-scale spatial resolution is set by the finite softening length which is introduced to avoid the formation of tight binary pairs which would force a significant decrease in the time step and lead to dramatic CPU requirements. Particle-Mesh codes have circumvented a number of those problems at the expense of the finite spatial resolution introduced by the existence of the grid system. The forces are interpolated from the grid and hence they are truncated on small scales. This helps to eliminate the two-body effects present in PP codes. Thus PM codes are well suited to the study of Vlasov-like systems where it is essential to suppress two-body effects, such as the dark matter density field in cosmological simulations. In an attempt to increase the spatial resolution of PM codes, Particle-Particle-Particle-Mesh (P^3M) codes were developed. P^3M codes are a hybrid class which use PM methods to compute large-scale forces and PP methods for small-scale interactions. This modification to PM codes partially helps to increase resolution. On the other hand they will suffer the same dramatic slow down which occurs with PP codes as clumping becomes significant. Furthermore, as emphasized by Sellwood (1987) P^3M codes may introduce two-body effects on small-scales thus making them unsuitable for use in modeling Vlasov-like systems. Pen (1994) has constructed a code which he refers to as a "Linear Moving Adaptive PM Code". This code is adaptive in the traditional sense, where the mesh spacing varies according to some local quantity, in his case the density. As a consequence of Adaptive Mesh Refinement (AMR) Pen finds that the particles in his code feel a self-force, this could be a problem for some

⋆ Present Address: Center for Computational Sciences, 325 McVey Hall, University of Kentucky, Lexington, KY 40506-0045 USA, randal@ccs.uky.edu

types of initial conditions. Katz & White (1993) introduced a "multi-mass" technique which is based upon the hybrid N-body/hydrodynamics code TREESPH, which was developed by Hernquist & Katz (1989). Katz & White (1993) used their "multi-mass" code to examine the properties of simulated galaxy clusters. In this method they use a series of nested lattices, with the particle mass growing smaller as one moves to more finely spaced lattices. Thus, they are able to obtain simultaneously high force accuracy and high mass resolution. This method is similar to the nested-grid methods that I will discuss next. In a similar spirit to P^3M codes where one increases the force resolution without concern for increasing mass resolution Suisalu & Saar (1995) and independently Jessop, et al. (1994) have developed multi-grid based adaptive particle codes. Both codes are capable of adaptively modifying the underlying grid to accommodate the varying distribution of particles. Suisalu & Saar (1995) use a full multi-grid method for the potential solver which is able to refine on regions of high density increasing their force resolution. Jessop, et al. (1994) use a relaxation Poisson solver and Neumann boundary conditions interpolated from the parent grid, coupled with a methodology for adaptively creating sub-grids in regions where increased force resolution would be of benefit.

Nested mesh codes have been available in the atmospheric sciences for a number of years, and Koch & McQueen (1987) provide a nice introduction. In these fields it was realized that nesting a fine mesh within a coarse mesh can be a very economical way to achieve higher resolution without increasing dramatically the required memory and CPU resources that an equivalent larger grid would need. Nested mesh techniques are one way to extend resolution in simulations of large-scale structure. Peebles (1980) first argued that long wavelength Fourier modes can couple to much shorter wavelength modes increasing the power on small scales. More recently Jain & Bertschinger (1993) have come to the same conclusion. As a consequence attempts to increase resolution by reducing the box size appear to be doomed from the start. Furthermore, moving from simple PM codes to P^3M codes on a similar sized grid appears to be capable of increasing the resolution by only a small factor, roughly a factor $O(10^3)$ shy of the required resolution for full simulations capable of addressing both the details of galaxy formation while still being able to follow the large wavelength modes.

Over the last several years a number of nested grid codes have been developed for use in cosmology and/or astrophysics. Chan et al. (1986) developed a nested mesh code for use in studying galaxy collisions. In the code of Chan, et al. the sub-grid potential is computed using a standard finite difference approach and the boundary conditions for the sub-grid are interpolated from the known coarse grid potential. Villumsen (1987) constructed a Hierarchical Particle Mesh (HPM) code which is similar to the code I will describe here. Recently, Anninos, et al. (1993) have reported a nested mesh code for use in cosmology which not only evolves the collisionless dark matter on a fine grid but performs a hydrodynamic calculation on the fine grid as well allowing them to follow both the dark matter and the baryonic matter component. The code developed by Anninos et al. is similar to that developed by Chan et al. in the sense that boundary conditions for the sub-grid region are obtained directly from the parent grid by interpolating potential values on parent mesh cells to the sub-grid. In a related approach to the nested grid schemes discussed above Couchman (1991) has modified the standard (P^3M) algorithm by introducing refined meshes in regions of high density. The traditional complaint against such codes has been that as clustering evolves they tend to slow down because there are an increasing number of particles within one cell of one another. This causes the PP step to become the dominant portion of the code and significantly slows down the code as a whole. To circumvent this, in regions of high density Couchman introduces refined meshes to guarantee that there is never a very large number of particles within the same grid cell. This prevents the PP portion of the code from dominating the overall runtime.

This implementation of a nested-grid algorithm has a number of advantages over the methods previously mentioned. Unlike codes such as P^3M, and tree codes I am able to get very high force resolution but without the slowdown associated in those codes for highly clustered distributions. Furthermore, I am able to not only increase the force resolution, but also the mass resolution on the sub-grid region. This is something which only other nested-grid codes are at present capable of doing. In comparison to the nested-grid codes, I feel that my mass advection scheme should make my method easier to generalize to a more adaptive scheme. I also enforce a Courant-Friedrichs-Levy (CFL) condition on the sub-grid time step, guaranteeing that the time integrator does not go unstable. This is contrary to the Villumsen (1988) version of a nested-grid code where no CFL condition is enforced on the sub-grid particles.

This paper is organized in the following way: section §II discusses in detail the algorithm that I have implemented, Section §III presents the results of a number of tests of the code, and finally in section §IV I present my conclusions.

2 GENERAL ASPECTS OF THE CODE

The general philosophy of the code is quite simple. I am free to define a sub-grid anywhere within the parent grid. As parent particles move into the sub-grid region I view them as consisting of n_{sg}^3 sub-grid particles which initially are on a cubic lattice the size of one parent grid cell. As the parent particle enters the sub-grid the sub-grid particles are free to move on a sub-grid mesh which is typically much finer than the parent mesh. This allows us to gain significantly better length resolution, albeit in a small localized region. Furthermore, since the typical sub-grid particle mass is $m_{sg} = m_{pg}/n_{sg}^3$, where m_{pg} is the parent particle mass I am able to gain additional mass resolution beyond that possible with the original PM code.

Up to this point the discussion has focused primarily on methods to increase force resolution. As emphasized by Melott & Shandarin 1989, and Melott 1990, increasing the force resolution is not enough in cosmological simulations. The authors argue that increasing the force resolution without a corresponding increase in the mass resolution will lead to the growth of spurious perturbations due to shot noise from the particles. As a consequence any method for increasing the force resolution without increasing the mass resolution will tend to lose phase information, and thus is not getting the physics correct in the model. Unfortunately, this

[t]

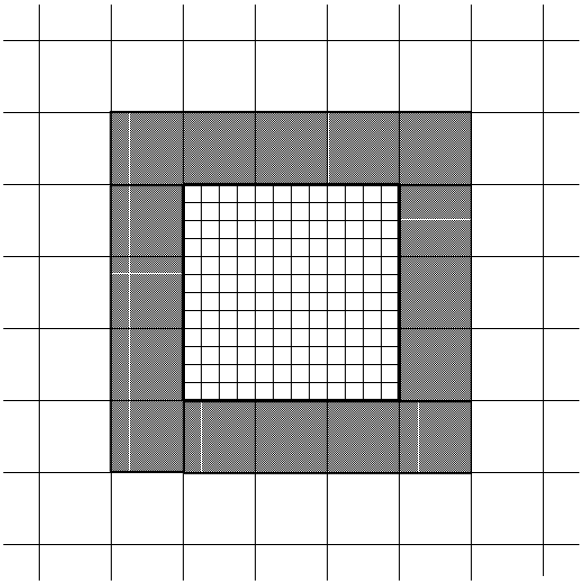

Figure 1. An example of the adjacent mesh structure that the nested mesh code utilizes.

error will not show up in the autocorrelation under most circumstances (Melott 1990). Therefore, results may very well be incorrect, but as long as the autocorrelation is being used to study the system the errors may not be apparent. One great advantage of a nested-grid scheme over other methods which try to increase the force resolution without increasing their mass resolution such as tree codes or P^3M, is that a nested-grid code will also increase the mass resolution since the sub-grid particles will always have a smaller mass than the parent grid particles. A nested-grid code will be capable of increasing force and mass resolution simultaneously, thus avoiding the introduction of any phase errors due to the growth of spurious perturbations in the simulation.

2.1 Grid Layout and Parent Grid/Sub-grid Interfaces

I have adopted an adjacent mesh structure, as discussed by Koch & McQueen (1987), for the sub-grid/parent grid hierarchy. A two-dimensional example is show in Fig. 1. I am free to define the size of the sub-grid in terms of parent cell sizes, once the coordinates of the lower left hand corner of the sub-grid have been stated. One can use an arbitrary number of parent grid cells and sub-grid cells, with a uniform spacing on both grids. In addition, the sub-grid region is fixed and is not allowed to move as the simulation progresses.

In my code a one-way interface is utilized so that the parent grid particles can influence the sub-grid particles, but the sub-grid distribution cannot back-react with the parent particles. Anninos et al. (1993) found that significant noise was generated when a two-way interface was used. As discussed by Koch & McQueen (1987) this may not be unreasonable to expect since the higher frequency waves present on the sub-grid may generate false waves at the interface, or since the high frequency waves cannot be represented on the much coarser parent grid they may lead to significant aliasing effects.

As emphasized by Koch & McQueen (1987) and Anninos et al. it is necessary to include a buffer zone around the sub-grid to smooth any density or force transients which may be introduced as the sub-grid particles enter the sub-grid region. I have found that a buffer zone the width of two parent cells is sufficient to minimize any transient effects from mass movement into or out of the sub-grid, but the width of the buffer zone is an input quantity and it can be varied if need be. In addition, the buffer zone is divided in half creating a inner and outer buffer zone. The sub-grid particles are moved using the parent grid potential until they enter the inner buffer zone. At that point the sub-grid particles are moved using the high resolution potential of the sub-grid region. The use of an inner and outer buffer zone helps the sub-grid particles to slowly relax to the additional power which the sub-grid potential possesses, and therefore by the time the sub-grid particles have reached the actual sub-grid they have relaxed and are moving under the influence of the sub-grid potential only. This helps to eliminate any edge effects which might come into play should the sub-grid particles not be allowed to relax prior to their entering the sub-grid region.

Furthermore, I have found the need to add a layer of 3 sub-grid cells in the buffer zone. Thus, increasing the mesh upon which the density assignment is performed by 6 grid cells in each direction so that the entire sub-grid is increased by two parent cells in all directions plus an additional 3 sub-grid cells in all directions. The addition of these extra sub-grid cells helps to guarantee that the advection of sub-grid particles into the sub-grid will not introduce any unwanted density fluctuations at the sub-grid/parent grid boundary. Details on how the forces are computed on particles as they move into the sub-grid region are given below.

2.2 Force Calculation

The forces on the parent particles are obtained by a simple two-point differencing of the potential on the parent grid. To obtain the forces on the sub-grid I break the calculation up into two stages (for a single nested mesh). First, I compute the density on the parent grid and set the density over the sub-grid region equal to the mean density on the sub-grid. By setting the density equal to the mean over the sub-grid region I erase all of the fluctuations on the sub-grid, but the total mass present on the sub-grid is still present. This density field is then Fourier transformed and convolved with the standard seven-point approximation to the Green function in k space, i.e.

$$G(\vec{k}) = \frac{\theta}{6 - 2\cos(\frac{\pi k_x}{L}) - 2\cos(\frac{\pi k_y}{L}) - 2\cos(\frac{\pi k_z}{L})} \qquad (1)$$

where θ is a dimensionless parameter defined to be $\theta \equiv 4\pi G\bar{\rho}\delta t^2$, and G is Newton's constant, $\bar{\rho}$ is the global mean density, δt is the magnitude of the time step. As discussed in Potter (1973) $\theta < 0.5$ for stability. I have chosen θ to be 0.49 .

When this potential is inverse Fourier transformed it represents the contribution to the subgrid potential from those parent particles which have not entered the subgrid. I then difference this potential and interpolate using a CIC scheme to compute the background forces on the subgrid particles. This leaves us with the final set of forces, the forces

[t]

Figure 2. A plot of the relative error between the Ewald generated Green function and the isolated Green function.

on the subgrid particles due to themselves. Here I use a transform technique similar to Villumsen (1989), but rather than imposing isolated boundary conditions on the subgrid potential I use "quasi-isolated" boundary conditions.

To test the relative error that would be made by using purely isolated boundary conditions as opposed to the "quasi-isolated" boundary conditions which I use in this code, I compute the relative error between the Ewald generated Green function and the isolated Green function. The horizontal axis is the quantity r/L where r is the radius and L the box size. The vertical axis is the relative difference between the Ewald Green function and the isolated Green function. Therefore for a sub-grid size which is 1/4 of the parent grid the the largest radius is $0.25\sqrt{3}$ and the error associated with using the isolated Green function rather than the Ewald Green function is roughly 40%. This plot is shown in Fig 2.

Eastwood & Browning (1979) and Hockney & Eastwood (1981) provide a method for imposing isolated boundary conditions on the a cubical mesh. I impose isolated boundary conditions on the sub-grid using the method discussed by the above authors. This consists of doubling the density field, padding the extra regions with zeros, and convolving it with a Green function which has an imposed periodicity of the main grid length. The Green function on the subgrid is computed using the Ewald method (1921) which possesses the full periodicity of the parent grid. In this manner I take into account the images of the sub-grid particles which would not exist if I used the Green function appropriate for an isolated system. This is what I mean by "quasi-isolated" boundary conditions. The Green function is computed once at the beginning of the simulation, transformed and saved. The transformed density is convolved with the Green function obtained from the Ewald method and Fourier transformed back to give us the high resolution subgrid potential. This potential can then be differenced and interpolated to obtain the sub-grid contribution to the forces on the subgrid particles.

Using the derivation of Ziman (1972) or Sangster & Dixon (1976) the Green function can be computed using the Ewald method. It takes the following form,

$$\begin{aligned} G(\vec{x},\vec{n}L) &= \frac{2\alpha}{\sqrt{\pi}} \\ &+ \frac{1}{\pi L}\sum_{\vec{h}}\cos(\frac{2\pi}{L}\vec{h}\cdot\vec{x})\frac{e^{-\pi h^2/L\alpha}}{h^2} \\ &+ \sum_{\vec{n}}\frac{1}{|\vec{x}-\vec{n}L|}\mathrm{erfcc}(\alpha|\vec{x}-\vec{n}L|) \end{aligned} \tag{2}$$

where $\vec{k} = 2\pi\vec{h}/L$, and $\vec{h}$ is an integer triplet, and α is an arbitrary parameter introduced by the Ewald method and represents the length scale at which the real and k space expansions become important. Hernquist et al. (1991) found adequate convergence when $\alpha = 2/L$, $|\vec{h}|^2 < 10$, and $|\vec{x} - \vec{n}L| < 3.6L$. I adopt their values in this code.

2.3 Time Integration

The time integration on both the subgrid and the parent grid is performed using a standard leap-frog technique. The advantages of using the leap-frog method are discussed in Hockney & Eastwood (1981) and Potter (1973). In order to ensure stability of the leap-frog integration I use separate time steps for the parent grid and the subgrid. I discuss this choice in more detail below. On the parent grid the time step is constrained first by a Courant-Friedrichs-Lewy (CFL) condition,

$$\delta t_{cfl} = 0.25 \times \frac{\delta x}{max|\vec{v}|}, \tag{3}$$

then secondly by a free fall time constraint

$$\delta t_{ff} = \frac{0.49}{\sqrt{4\pi G a^2 \rho_{max}}}. \tag{4}$$

The parent grid time step is then defined to be the minimum of the above two estimates $\delta t_{pg} = \min(\delta t_{cfl}, \delta t_{ff})$. On the subgrid the same two quantities are computed and the minimum of the two chosen, δt_{sg}. Then I compute their ratio and truncate it. This is the number of subgrid steps,

$$N_{steps} = \mathrm{int}(\delta t_{pg}/\delta t_{sg}), \tag{5}$$

I am allowed to take before I must take another parent step to update the parent grid potential. Then the actual subgrid time step size is chosen to be $\delta t_{sg} = \delta t_{pg}/N_{steps}$.

The use of asynchronous time steps for the sub-grid particles is an improvement over using the same time step for both grids. The reasons for that are straightforward. I have chosen to use the leap-frog integration scheme to perform the time integrations, therefore I must enforce a CFL condition on both the sub-grid and the parent grid. This is to guarantee the stability of the time integration. At this point several approaches could be used. The first would be to compute the most restrictive time step on both the sub-grid and the parent grid from the CFL conditions on each, and evolve both meshes using the same time step. This would lead to large overhead since the sub-grid time step will nearly always

be much smaller than the parent time step, thus forcing me to evolve the parent grid particles for many more time steps than is needed for an accurate solution. Secondly, I could use asynchronous time steps, updating the parent particles only when necessary. I can justify the use of an asynchronous time step by the following two arguments. First the gravitational infall timescale should be an estimate of the dynamical timescale for the system. Since the gravitational infall timescale is proportional to the inverse of the square root of the density, and since I have much higher mass resolution on the sub-grid I expect much smaller infall timescales for the sub-grid, in other words the sub-grid particles should be evolving on a smaller timescale. Thus to accurately follow their motion I need a smaller time step. A second justification for the use of asynchronous time steps is also possible using several recent approximation methods. Based upon the work of Brainerd et a. (1993) and Bagla & Padmanabhan (1994) on the 'Frozen Potential' formalism we know that the potential does not vary too much over the course of evolving the model. Furthermore, Melott et al. (1995) argue in their 'Stepwise Smoothed Potential' formalism that gravitational clustering is equivalent to smoothing the initial potential on increasing scales. As a consequence objects which are distant and have been smoothed will tend to have a small effect on the evolution of the sub-grid distribution of particles. Thus, I should be able to evolve the sub-grid distribution separately from the parent grid safely.

2.4 Mass Advection

Crucial to any nested mesh code is how one deals with the advection of mass into the subgrid region. The technique that I have chosen to use is significantly different than either Villumsen (1987) or Anninos et al. (1993) who perform a background run with only parent particles, tag the parent particles which actually enter the subgrid then during a subsequent run they evolve the distribution of parent particles and the subgrid particles whose parents will eventually enter the subgrid. Prior to the subgrid particles entering the subgrid they are moved using the background potential used to move the parent particles. Then upon entering the subgrid the finer subgrid potential with its higher Fourier components is used to move the subgrid particles. A possible disadvantage of this method is that one must evolve the full distribution of sub-grid particles, both those particles on the sub-grid and those that have not yet entered the sub-grid. I believe that my scheme is significantly better, because I avoid the overhead entailed by evolving those sub-grid particles not on the sub-grid is nonexistent, and since the subgrid particles do not exist until they are laid down on the sub-grid region my method will make it significantly easier to generalize my code to a fully adaptive setting where the code defines local sub-grid regions on its own for refinement and subsequently lays down the sub-grid particles without the need for running the code multiple times refining in a local region each runtime.

The method I use for laying down the sub-grid particles is somewhat similar to how particles are smeared out in a anisotropic manner in adaptive or tensor smooth particle hydrodynamics algorithms (Martel et al. 1994, or Benz & Davies 1993). As the parent particles approach the buffer zone I consider their volume as having been smeared out in space, with the cloud for a parent particle being given by half the distance to the nearest parent particle in that particular direction. As a consequence as far as the sub-grid particle advection algorithm is concerned the parent particles no longer have a volume equal to a parent grid cell cubed. In essence I am distorting the volume of the sub-grid particle cloud in phase space to be consistent with the phase space distortions of the parent particles. Once the characteristic size of the parent particle is known the coordinates of the sub-grid particles can be computed simply, assuming that they are laid down uniformly in each direction.

The x, y, and z components of the velocity are then assigned by performing a multivariate interpolation between the nearest 3^3 parent particles in phase space in each direction. The interpolation algorithm I use was developed by Renko (1988). It is a multivariate interpolation scheme which is capable of performing the interpolation on scattered data points. Then the subgrid particles are moved using only the parent potential until they reach the edge of the buffer zone discussed above at which point they are moved using the high-resolution potential generated on the subgrid. This should be adequate for most problems of interest, and the following tests demonstrate that little significant error is introduced in the evolved sub-grid particle distribution. Furthermore, I believe the strength of my technique is that it should generalize to a fully adaptive nested grid code somewhat easier than the Villumsen (1988) algorithm which requires they be laid down before evolution of the distribution begins.

3 INITIAL CONDITIONS

It has become standard place in cosmological simulations to generate initial conditions by using the Zel'dovich (1971) approximation. The Zel'dovich approximation was first used to by Klypin & Shandarin (1983), and Efstathiou et al. (1985) to generate the initial conditions for the particles in a cosmological simulation. Randomly generated initial particle positions generate shot-noise in the initial density fields on all scales. In models close to equilibrium at the beginning, the initial behavior is dominated by the collective response to this initial noise, thus masking the true modes of the system. Traditionally this noise has been reduced by turning to *quiet starts* to generate initial conditions. Byers and Grewel (1970) showed that arranging the particles uniformly at the outset suppressed the amplitude of spurious density fluctuations due to shot-noise. Further, provided there are at least as many particle planes as there are grid spaces in each direction Melott (1983) and Efstathiou et al. (1985) showed that a regular grid spacing in each coordinate direction will give a quiet start to a cosmological simulation on a Cartesian grid.

The initial conditions for the parent particles are generated in the standard way: the particles are laid down on a uniform mesh and then perturbed away from the uniform mesh through the use of the Zel'dovich approximation (1970) which requires the initial power spectrum for the density perturbations. The use of a uniform mesh ensures that the shot-noise fluctuations in the density will be minimized. The resulting density perturbations are consistent with the initial power spectrum with random phases.

Villumsen (1989) has discussed a method for generating power on scales not resolvable by the parent grid. I have begun writing such a code and will present the tests of the method in an upcoming paper, and focus only on the evolution code in this paper.

4 CODE TESTS

In this section I wish to present a number of tests of the code.

4.1 Force/Potential Accuracy

The first non-trivial test, compares the accuracy of the forces on the parent grid and on the sub-grid. One parent particle is laid down the parent grid with the $4^3 = 64$ sub-grid particles laid down at the same grid location on the sub-grid. The sub-grid is chosen to be five parent cells on a side with 25^3 mesh cells for a refinement factor of five, and a sub-grid mesh size of 0.2. The peculiar choice for the number of sub-grid cells is made so that the 64 sub-grid particles lie in one sub-grid cell only and are not smeared over the eight nearest neighbors when the density assignment is performed. The density fields are computed on each grid, and the corresponding potential field is computed for each grid. Then the forces are computed at 2000 randomly chosen positions on each grid. The results are plotted in Fig. 3, the small dots are the forces from the parent grid, the open circles are the forces determined for the refinement given above, and the filled circles are the forces for a refinement factor of 15. I note several things concerning this result. First, both force fields have roughly the resolution expected; the parent grid forces go too soft at a radius of roughly 1, where I would have expected them to, and the sub-grid forces go too soft at roughly a radius of 0.2, again exactly where I would have expected them to. Secondly, the sub-grid forces appear to be much more isotropic than the parent grid forces, as measured by the typical scatter of the points at a given radii. Finally the force resolution on the sub-grid appears to scale correctly as one increases the resolution of the code.

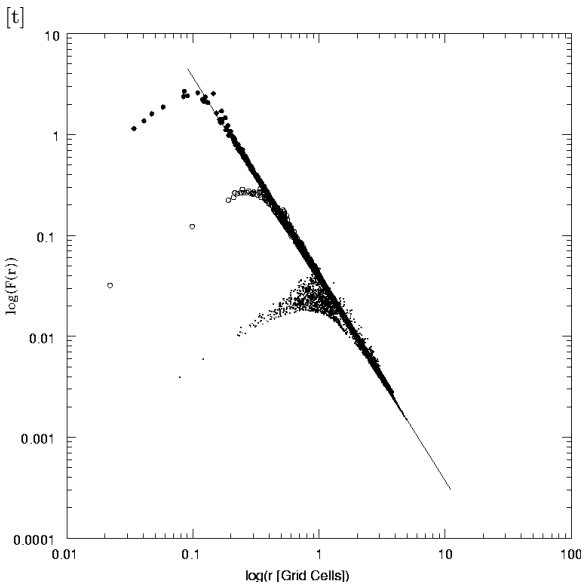

Figure 3. A plot of the sub-grid and parent grid force resulting from a single particle. The parent grid forces are given by the dots, the open circles give the sub-grid forces for a refinement of 5, the solid circles give the sub-grid forces for a refinement of 15, and the solid line gives the exact analytical solution from the Ewald method.

4.2 Plane Wave Collapse - The Zel'dovich Approximation

The simplest and most straightforward test is a one dimensional test which is useful since it possesses an analytic solution. The analytic solution was completed by Zel'dovich in 1970, and has come to be known as the Zel'dovich approximation. The test has been performed with the perturbations aligned along the x axis similar to Efstathiou, et al. (1985) for a strict PM and P^3M code. To make the test more challenging I run the test with the perturbation moving diagonally from lower corner to the diametrically opposite corner of the box. For this test the code was evolved to a $\delta_{rms} \approx 1.0$, where δ_{rms} is the RMS variation of the global density field. I chose to run the code only up to a $\delta_{rms} \approx 1.0$ because the Zel'dovich approximation breaks down at that point, making a comparison to the approximation impossible. At the same time spurious velocities in the two orthogonal directions were about $\bar{v}_{y,z} \simeq O(10^{-3})$, which, when multiplied by the total runtime of the simulation, corresponds to spurious particle motion in the two orthogonal directions of less than 1/30th of a subgrid cell. Fig. 4 shows a phase space plot; the open squares are the parent grid particles, and the solid dots are the sub-grid particles. To generate this plot I project the particle positions onto the plane which runs diagonally through the box. I do not include the analytic fit because it would obscure most of the sub-grid points. Fig. 5 shows the density field for that same simulation. To make this plot I simply plotted the density in the cells along the diagonal of the box. This spurious motion is unavoidable given my use of quasi-isolated boundary conditions on the sub-grid. Furthermore it contributes to the slight appearance of noise that is seen in the phase space plot. Nonetheless, the motion appears to be a small perturbation on the overall collapse of the pancake, and thus the effect appears to be negligible.

4.3 Spherical Infall

For any code, comparison with known analytic results is paramount. Furthermore, tests which possess a symmetry not intrinsic to the code are of particular usefulness. In the spherical infall test I have both such cases. The code with its cubic cells may tend to favor tests which may possess planar symmetry such as the plane wave test above. The analytic solution to spherical infall was worked out in detail by Fillmore & Goldreich 1984, Bertschinger (1985). Bertschinger found for small values of the radius the solution approached a power law form. In this test a uniform distribution of particles was laid down on both the parent grid and the sub-grid. Then I took several time steps in which the density field was given by the CIC values from the particles plus an extra particle on the parent grid and 64 extra particles on the sub-grid to serve as seed masses to start the infall. The parent seed mass and the sub-grid seed masses all had

[t]

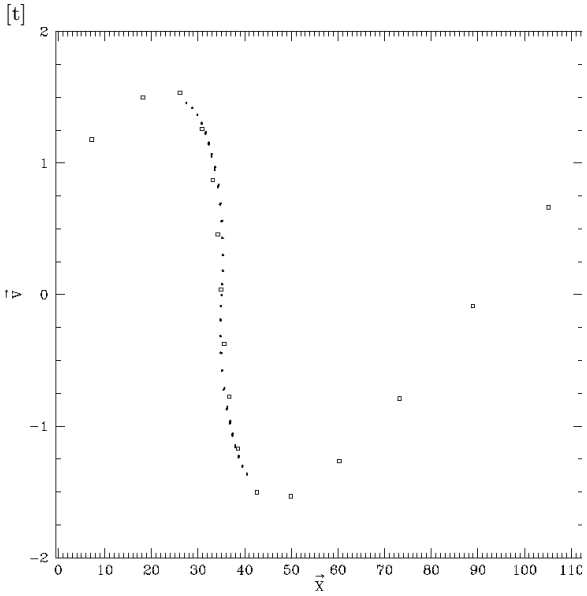

Figure 4. A phase space plot of the parent grid, and sub-grid particles. The open squares are the parent grid particles while the open circles are the sub-grid particles. This model was evolved up to the onset of non-linearity, $\delta_{rms} = 1.0$.

[t]

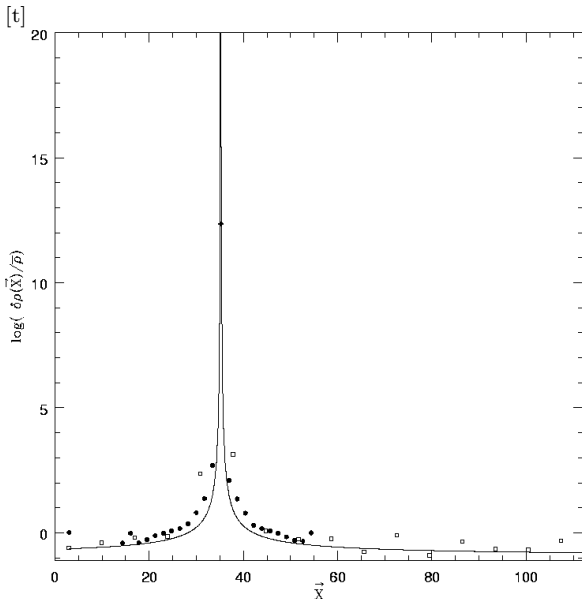

Figure 5. A plot of the evolved density field on the parent grid and the sub-grid at the onset of non-linearity in a 1D collapse model. No discernible noise can be detected in the sub-grid density due to my method of laying down sub-grid particles. The filled in circles are the sub-grid densities, while the open boxes are the parent grid solution.

the same coordinates to guarantee that the infall was symmetric with respect to the same point on both grids. After several time steps with this *perturbed* density field the extra seed masses were removed and the particles were allowed to move based upon the CIC derived density field and the resulting potential. The sub-grid was chosen to be 5 parent grid cells in size with 25^3 sub-grid cells. This implies that I can expect about a factor of 5 increase in resolution.

[t]

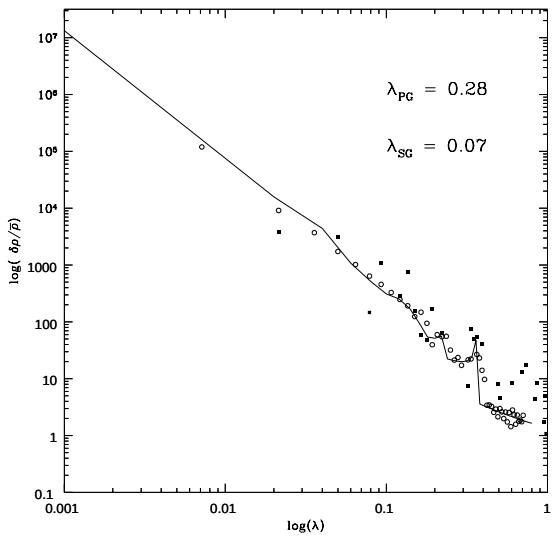

Figure 6. A comparison of the computed density profiles from the nested grid code to the analytic solution. The solid line is the analytic solution while the open circles are the sub-grid solution, and the filled in boxes are the parent grid solution.

The amplitude is fixed uniquely by specifying the radius at turnaround, Peebles et al. (1989). Furthermore they were able to show given an initial mass perturbation m_0 then the turnaround radius, r_{ta} is given by

$$m_0 = \frac{9\pi^3}{80}(6\pi)^{2/3}\rho_b r_{ta}^3. \tag{6}$$

Therefore once r_{ta} has been determined, then the dimensionless radius, $\lambda = r/r_{ta}$, can be specified and the normalization of the density profile is set. For this test $r_{ta} \approx 3.5$ parent grid cells.

To determine the density profile from the particle positions I bin the particles into spherical shells, this gives the number density of particles as a function of radius. In the case of the parent particles this is the density profile $(\rho(r) - \bar{\rho})/\bar{\rho}$, but in the case of the sub-grid particles this is just the number density at radius λ. To get $(\rho(r) - \bar{\rho})/\bar{\rho}$ for the sub-grid I must divide the number density by the number of sub-grid particles per parent particle, this corrects for the n_{sg}^3 sub-grid particles which comprise each parent particle. This result gives us the final density distribution.

Fig. 6 is a plot of the evolved density profile for the spherical infall problem. In Fig. 7 and 8 I show a dot plot of the particle positions within the sub-grid region. Fig. 7 shows the particle locations on the parent grid for a slice 2 parent cell in thickness, while figure 7 shows the particle positions on the sub-grid 1/4 a parent cell in thickness. In each dot plot one can clearly see spherical shells. The sub-grid solution has some slight deviations from perfect spherical symmetry near the central peak. These deviations could be due to my mass advection scheme, and the fact that as the particles enter the sub-grid region the interpolation used to assign sub-grid particle velocities is in error by a small amounts. Thus the particles are moving in slightly the wrong direction. The effect is small as evidence by the accuracy of the density profile, to be considered in Fig 6.

[t]

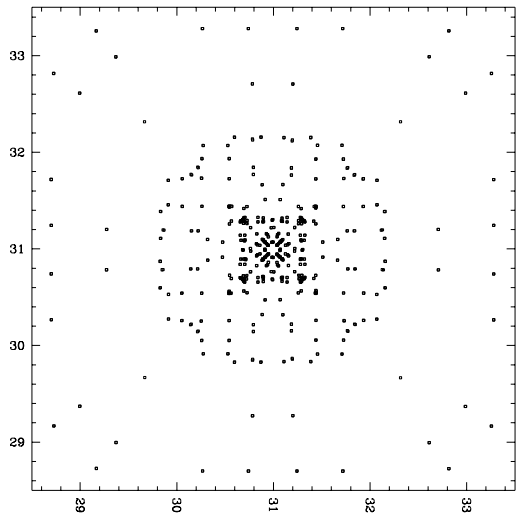

Figure 7. A slice plot showing the parent particle positions on the sub-grid region for a slice two parent cell in thickness.

[t]

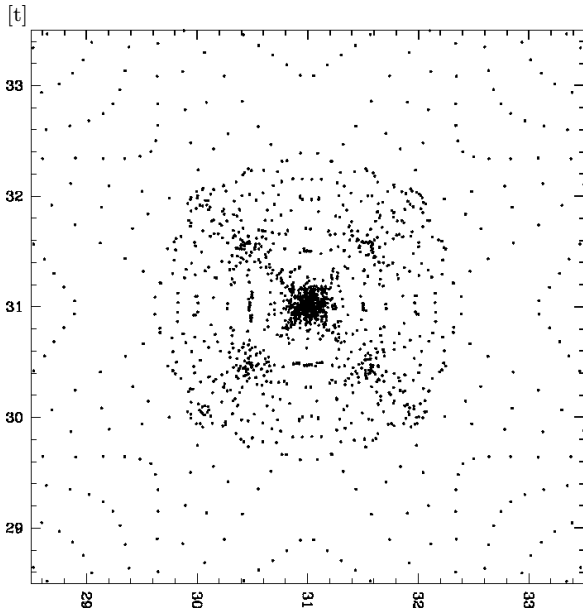

Figure 8. A slice plot showing the sub-grid particle positions on the sub-grid region for a slice 1/4 parent cell in thickness.

The solid line is the Bertschinger analytic solution, the open squares are the density profile of the parent particles, and the crosses are the sub-grid density profile. There is some deviation from the analytic solution for the parent particles which is expected since I am using a relatively coarse grid for this calculation. The sub-grid appears to agree favorably with the analytic solution down to values of $\lambda \simeq 0.007$, which corresponds to roughly a length of one-sixth of a sub-grid cell. Thus, I appear to be obtaining better resolution than one would naively expect from a particle-mesh type code, where I would expect the sub-grid solution to be valid only down to scales of one sub-grid cell over r_{ta}, or 0.07. In addition, the sub-grid solution appears to be roughly a factor of 10 better than the parent grid solution. Indicating that I am getting better resolution on the sub-grid by roughly a factor of 10, when naively based upon the cell sizes on the parent grid and sub-grid I would only expect a factor of 4 in improvement.

4.4 Spherical Hole

Another test of how well the code is able to evolve systems whose inherent symmetry differs substantially from cubic is the spherical hole solution due to Fillmore & Goldreich 1984), and Bertschinger (1985). For this test I run the code with a single sub-grid centered on an uncompensated hole. Bertschinger (1985) showed that the central void should grow as $R \propto a^n$, where $n = 1/5$. I ran simulations using a 16^3 grid with the same number of parent particles on the grid. The parent particles and sub-grid particles were then binned into spherical shells to compute the density profiles. From the profiles I find $n = 0.182 \pm 0.022$, consistent with the theoretical result of Bertschinger.

4.5 Two-Dimensional Perturbations

For the final test of the code I compare the results of a 512^2 two-dimensional simulation to the evolution of the same initial conditions using my 3D nested-grid code. For this test one of the 2D models from Beacom, et al. (1991) was used. This model has an initial power-law density fluctuation spectra, with a spectral index of 0, and a high frequency cutoff at $k = 32$. This choice of cutoff was made so that initially there would not be any power in the Fourier modes which can only be felt on the sub-grid. Thus, any clustering on the sub-grid region will be purely a consequence of evolution.

The following test is different from the previous test cases. In all the previous tests there exists an analytical solution to the test. Unfortunately all of the analytic solutions possess certain symmetries. It is likely that a real model will not possess many of the symmetries which have been discussed to this point. As a consequence if I wish to compare solutions to my nested-grid code to more realistic cases I must compare to 2D solutions rather than full 3D. This is due to the lack of dynamical range in the 3D simulations. The 2D code used here for comparisons has been well tested in the work of Beacom, et al. (1991), and provides a useful benchmark for more sophisticated testing.

Based upon the final evolved distribution of particles in the 2D model, I identify a sub-grid region. Then all of the particles which enter the sub-grid are tagged. These particles will become the initial distribution of sub-grid particles. The full 512^2 distribution is then sampled every fourth particle to reduce it to a 64^2 set of particles. These become the parent grid particles. The 64^2 distribution of parent particles are laid down onto a 64^3 grid. I then define a sub-grid region which has the same resolution as the initial 512^2 mesh. The nested-grid code is then run up to the same non-linear wavelength, in this case $k_{nl} = 4$, as extrapolated from linear theory.

I can then compare the distribution of particles in the

sub-grid region of the original 2D data set to the evolved distribution of sub-grid particles on the sub-grid region of the full 3D simulation. I should find that the two distributions agree nicely. Furthermore, I can use this as a test of collisionality, because as particles accrete onto one of the clumps in the sub-grid they should not scatter out of the plane. Hence in the final 3D distribution none of the sub-grid particles should have acquired a velocity component in the $\hat{z}$ direction.

Fig. 9 is a 64^2 sub-sample of the full 512^2 final evolved particle distribution for the original 2D perturbations. The left hand column contains the original 2D particles while the right hand column contains the particles from the nested-grid 3D simulation. The top left is the evolved 2D distribution plotting every 8th particle. The top right is a slice through the parent grid plotting only the sub-grid region. The bottom left is the full set of 2D particles on the sub-grid region, while the lower right is the evolved sub-grid distribution. The bottom two dot pictures of the sub-grid region agree nicely with only a slight indication of edge effects. Furthermore by comparing the plot in the upper right to the plot in the lower right hand corner one can get a perspective on the effect of increasing the mass resolution.

I compare the initial z positions of the particles to the evolved z positions of the particles by computing the mean of the absolute value of their difference. I find the motion in the z direction to of order $1/250th$ of a sub-grid cell, and thus is completely negligible. There is no motion on the parent grid down to round-off level. This indicates that the quasi-isolated boundary conditions I apply to the sub-grid region introduce little noise in the form of sub-grid particle motion out of the plane of the initial 2D perturbations.

To make the comparison between the dot plots in Fig. 9 more qualitative I compute the correlation coefficient between the density field on the 2d sub-grid region and the density field on the 3D sub-grid. To generate a 3D density field from the 2D particle positions I extract all particles on the sub-grid region plus a small buffer to minimize edge effects and stack the appropriate number vertically to make the density field three-dimensional. The correlation coefficient is defined to be

$$K = \frac{< \delta\rho_{2D}(x)\delta\rho_{SG}(x) >}{\sigma_{2D}\sigma_{SG}}, \tag{7}$$

where $\delta\rho_{2D}$ is the density field generated from the 2D distribution, $\delta\rho_{SG}$ is the density field generated from the sub-grid distribution of particles, and σ_{2D}, and σ_{SG} are the standard deviations of the respective density fields. For the model considered here I find K = 0.98. Thus I have quite good agreement between the original 2D density field and the full 3D sub-grid density field.

4.6 3D Mass Advection Test

Based upon the 1D Zel'dovich test it is clear that the sub-grid particles are being advected into the sub-grid region correctly when there is little clustering in the sub-grid region. Now I wish to test if the same conclusion holds when there is clustering of the parent grid particles prior to the sub-grid particles being created on the sub-grid. There is to my knowledge no analytic solution for such a problem. At the request of the referee I am providing this additional test of the advection scheme which I am using for the sub-grid particles. This test has no known solution and so I will be looking for any significant deviations which might be introduced by the advection scheme. As I will demonstrate I am unable to find any such effects.

To begin the test I use a 32^3 parent mesh with the same number of particles. The initial spectrum on the parent grid is scale-free and has a spectral index of -1. I evolve the system to a non-linear wavenumber of 2 performing data dumps at $k_{nl} = 16, 8, 4$, where k is measured in units of the fundamental. Then based upon the $k_{nl} = 4$ model I find a region where a merger has recently taken place between two clumps. I define a sub-grid region there and evolve the parent grid particles and the sub-grid particles, again perfomring data dumps at the same non-linear wavenumbers. In figure 10 I have plotted a series of dot plots through the sub-grid region. The right-hand column is the sub-grid grid particles and the left-hand plots are the parent particles. The top row are the particle positions at $k_{nl} = 16$, the middle row at $k_{nl} = 8$, and the bottom row is at $k_{nl} = 4$. In all cases the sub-grid distributions appear to be consistent with the parent grid particles.

Once again to make the arguement more qualitative I compute the density cross-correlation function between the sub-grid particles and the parent particles in several ways. First I extract all the parent and sub-grid particles within the sub-grid region plus a small buffer to avoid edge effects. I bin both sets of particles onto a mesh the same resolution as the parent mesh. I then cross-correlate these density fields. These results are in column 2 of table 1, and are labeled K_{SG}. The third column of table 1 contains the cross-correlations cimputed in a slightly different manner. Since I know from which parent particle each sub-grid particle came, I can compute the center of mass of the cloud of sub-grid particles for each parent particle on the sub-grid. I then bin these centers of mass onto a mesh with the same resolution as the parent mesh. I then compute the cross-correlation between this new density field obtained from the sub-grid particle centers of mass and the parent grid particles as before. These cross-correlations are in column 3 of table 1, and are labeled K_{CM}.

There is relatively good agreement in all cases. Of course I don't expect the cross-correlation to be exact. The sub-grid has much higher resolution than the parent grid so the sub-grid particles will have small scale motions which will cause deviations in their motions from what one would expect without higher force resolution. Furthermore, the agreement between the sub-grid distribution and the parent grid distribution gets poorer as the models evolve further. This is to be expected due the presence of small scale motions on the sub-grid which cannot be resolved on the parent grid. In addition, the second set of cross-correlations is better than the first which again is to be expected since the center of mass of a cloud of sub-grid particles should remain reasonably close to the location of the corresponding parent particle. Any deviations will be due to the small scale motions which can exist on the sub-grid and not the parent grid. All of this is consistent with the results of Melott & Shandarin (1993), who find that if one computes the cross-correlation between models whose only difference is the cut-off scale k_c then in the limit that $k_{nl} << k_c$ the difference between the two models should become negligible.

5 ACKNOWLEDGMENTS

I would like to thank NASA for support through a NASA Graduate Student Fellowship, NGT50816, the National Science Foundation (AST-9021414), my thesis advisor Adrian L. Melott for many valuable discussions, and Jennifer Pauls, Capp Yess, and Sergei Shandarin for a critical reading of the manuscript prior to submission. All calculations were performed at the National Center for Supercomputing Applications in Urbana, Illinois.

REFERENCES

Anninos, P., Norman, M., Clarke, D.A. 1994, ApJ, 436, 11
Aarseth, S.J. 1985, in Brackbill, J.W., Cohen, B.J., eds, Multiple Time Scales, Academic, New York
Bagla, J.S., Padmanabhan, T. 1994, MNRAS, 266, 227
Beacom, J.F., Dominik, K.G., Melott, A.L., Perkins, S.P., Shandarin, S.F. 1991, ApJ, 372, 51
Bell, J., Berger, M.J., Slazman, J., Welcome, M. 1992, LLNL Preprint
Benz, W., Davies, M. 1993, in Wingate, C., Miller, W., eds, Workshop on Advances in Smooth Particle Hydrodynamics, unpublished
Bertschinger, E. 1985, ApJS, 58, 39
Brainerd, T.G., Scherrer, R.J., Villumsen, J.V. 1993, ApJ, 418, 570
Byers, J.A., Grewel, M. 1970, Phys Fluids, 13, 1819
Chan, K.L., Chau, W.Y., Jessop, C., Jorgenson, M. 1986, in Hut, P., McMillan, S., eds, The Use of Supercomputers in Stellar Dynamics, Springer-Verlag, Berlin
Couchman, H.M.P 1991, ApJ, 368, L23
Doroshkevich, A.G., Kotok, E.V., Novikov, I.D., Polyudov, A.N., Shandarin, S.F., Sigov, Yu. S. 1980, MNRAS, 192, 321
Efstathiou, G., Davis, M., Frenk, C.S., White, S.D.M. 1985, ApJS, 292, 371
Elsberry, R.L., Ley, G.W. 1976, Mon Wea Rev, 104, 797
Ewald, P.P. 1921, Ann Phys, 64, 253
Fillmore, J.A., Goldreich, P. 1984, ApJ, 281, 1
Fillmore, J.A., Goldreich, P. 1984, ApJ, 281, 9
Garabedian, P.R. 1964, Partial Differential Equations, Wiley, New York
Hernquist, L., Bouchet, F.R., Suto, Y. 1991, ApJS, 75, 231
Hernquist, L., Katz, N. 1989, ApJS, 70, 419
Hockney, R.W., Eastwood, J.W. 1981, Computer Simulations Using Particles, McGraw-Hill, New York
Eastwood, J.W., Browning, D.R.K. 1981, J Comp Phys, 32, 24
Jain, B., Bertschinger, E. 1993, Preprint
Jessop, C., Duncan. M., Chau, W.Y. 1994, J Comp Phys, 115, 339
Katz, N., White, S.D.M. 1993, ApJ, 412, 455
Klypin, A.A., Shandarin, S.F. 1983, MNRAS, 204, 891
Koch, S.E., McQueen, J.T. 1987, NASA Technical Memorandum 87808
Martel, H., Shapiro, P.R., Villumsen, J.V, Kang, H. 1994, Preprint University of Texas, McDonald Observatory
Melott, A.L. 1983, MNRAS, 202, 595
Melott, A.L. 1990, Comments Astrophys, 15, 1
Melott, A.L., Sathyaprakash, B.S., Sahni, V. 1995, Preprint astro-ph 9504087
Melott, A.L. Shandarin, S.F. 1989, ApJ, 343, 26
Melott, A.L. Shandarin, S.F. 1993, ApJ, 410, 469
Peebles, P.J.E. 1980, The Large-Scale Structure of the Universe, Princeton University Press, Princeton
Peebles, P.J.E. 1987, ApJ, 17, 576
Peebles, P.J.E., Melott, A.L., Holmes, M.R., Jiang, L.R. 1989, ApJ, 345, 108
Pen, Ue-Li 1994, Preprint Princeton University Observatory
Potter, D. 1973, Computational Physics, Wiley, New York
Renko, R. 1988, ACM TOMS, 14, 139
Sangster, M.J.L., Dixon, M. 1976, Adv Phys, 25, 247
Sellwood, J.A. 1987, ARA&A, 25, 151
Suisalu, I., Saar, E. 1995, Preprint
Villumsen, J.V. 1988, ApJS, 71, 407
Ziman, J.M. 1972, Principles of the Theory of Solids, Cambridge University Press, Cambridge
Zel'dovich, Ya. B. 1971, A&A, 5, 84

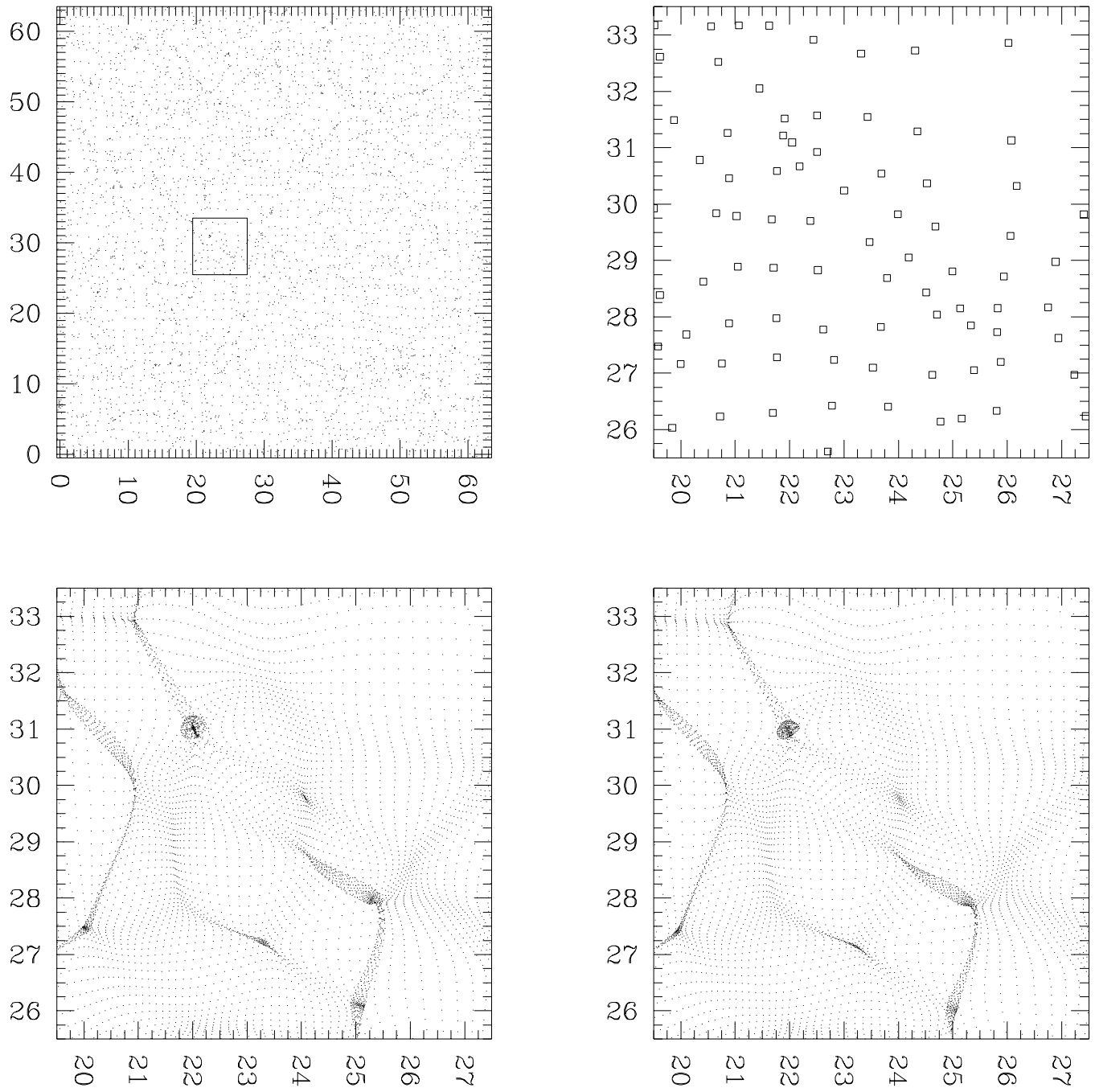

Figure 9. A dot plot of a slice through the distribution of particles in the 2D perturbations test. The left hand column contains the original 2D distribution, and the right hand column contains the 3D distribution from the nested-grid code. The upper left plot is the evolved distribution of particles in the 2D case, where only a 64^2 subset of the original 512^2 particles has been plotted. The small box labels the position of the sub-grid region with the parent grid. The upper right is a slice through the sub-grid region of the parent grid particles. The lower left is the evolved distribution of particles from the 2D distribution on the sub-grid region. The lower right is the evolved distribution of sub-grid particles. The small boxes in the upper left plot labels the sub-grid region.

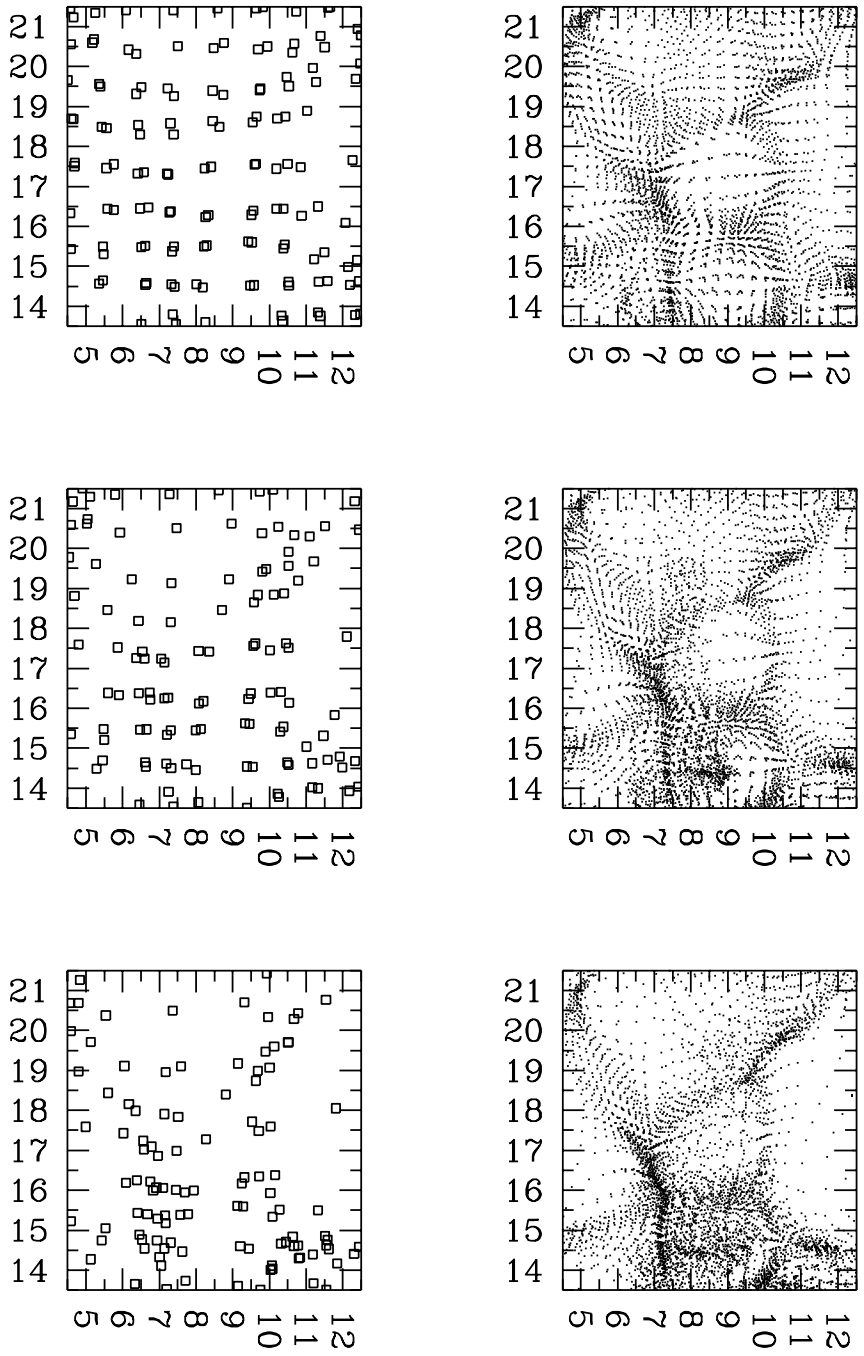

Figure 10. The left-hand column contains plots of the parent particles in a slice 2 parent grid cells thick. The right hand column is the sub-grid particle positions in a slice 1 parent cell in thickness. The top row are the particle positions at $k_{nl} = 16$, the middle row are the particles at $k_{nl} = 8$, and the bottom row are the particles at $k_{nl} = 4$.

Table 1. Cross-Correlations from the 3D Mass Advection Test

k_{nl}	K_{SG}	K_{CM}
16	0.942	0.971
8	0.893	0.942
4	0.874	0.897